Advances in Concrete Construction, *Vol. 19, No. 3 (2025) 151-162*
https://doi.org/10.12989/acc.2025.19.3.151

Behavior analysis of waste fiber-reinforced recycled concrete columns under axial and eccentric compression

Tianbei Kang*[1,2,3], Ping Zhang [1a], Jinghai Zhou [3b] and Yanfeng Li [4c]

[1] *School of Civil Engineering, Shenyang Jianzhu University, Shenyang, P.R. China*
[2] *Shenyang Key Laboratory of Low-carbon Transportation Construction, Maintenance and Operation, Shenyang Jianzhu University, Shenyang, P.R. China*
[3] *Green and Livable Rural Construction Institute, Shenyang Jianzhu University, Shenyang, P.R. China*
[4] *School of Transportation and Geomatics Engineering, Shenyang Jianzhu University, Shenyang, P.R. China*

(*Received April 25, 2023, Revised February 2, 2025, Accepted February 23, 2025*)

Abstract. This study was determined the impact of recycled coarse aggregate content (0%, 50%, and 100%), waste fiber length (12, 19, and 30 mm), volume fraction of waste fibers (0.08%, 0.12%, and 0.16%), slenderness ratio (2, 5, and 8), and eccentricity (0, 30, and 60 mm) on the bearing capacity of concrete columns. The results indicated that the cracking load and ultimate bearing capacity of waste fiber recycled concrete (WFRC) column decrease as the replacement rate of recycled aggregates increases, and initially increase before decreasing with the increase in both the length and content of waste fibers. The highest bearing capacity is achieved when the waste fiber length is 19 mm with a content of 0.12%. The waste fibers exhibit superior bond strength with the concrete matrix and effective load transfer, which inhibit the development the cracks during the loading process and improve the bearing capacity of the specimens. Additionally, the experimental results of WFRC were compared with the theoretical values calculated according to the "Code for Design of Concrete Structures" GB50010-2010, the ratios of the calculated value to the experimental value in the range of 0.81–1.10. The feasibility and safety of the related properties of the WFRC column according to the results calculated by the standard GB50010-2010. The standard GB50010-2010 can guide the application design of WFRC compression members in practical engineering.

Keywords: axial compression; column; eccentric compression; recycled aggregates; waste fibers

1. Introduction

With population growth and urbanization, concrete consumption has increased sharply. Recently, 2.4 billion tons of concrete have been produced in China (Shen *et al*.2017). Demolition of buildings produces large amounts of waste, and the environmental pollution caused by non-renewable resources, such as sand and stone, consumed for concrete production is also inevitable (Yazdani *et al*. 2021). The use of new energy-saving and environmentally friendly building materials and structures can significantly enhance the development of the construction industry (Naran *et al*. 2022). Therefore, the production of recycled coarse aggregate (RCA) concrete has decelerated the consumption of natural resources, while ongoing consumption of vast amounts of construction and demolition waste.

The surface of RCA is attached to the old mortar, which results in the characteristics of more interfacial transition zone, higher porosity, and higher crushing index than that of natural coarse aggregate (NCA). These features lead to a higher water absorption rate and lower apparent density of RCA concrete compared to NCA concrete (Strieder *et al*. 2022, Yaragal *et al*. 2016). As the replacement rate of recycled aggregate increases, both the strength and durability of concrete tend to degrade (Poon *et al*. 2004, Kang *et al*. 2022a). Columns are indispensable parts of industrial and civil buildings, and scholars have conducted a series of studies on the mechanical properties of RCA columns. Research indicates that the RCA replacement rate and RCA type will affect the non-axial compressive performance of RCA concrete columns (Gao *et al*. 2021, Ma *et al*. 2019). The higher the replacement rate of RCA, worse the compressive capacity of the columns (Zhao *et al*. 2022). The axial compressive performance of the RCA concrete column is the same as that of the NCA concrete column, and can be divided into cracking, yield, ultimate load, and failure stages, respectively (Liu *et al*. 2019). The damage and surface cement peeling of RCA concrete columns occur earlier than those in NCA concrete columns because the splitting tensile strength of RCA concrete is worse than that of NCA concrete (Sunayana and Barai 2019). In summary, the bearing capacity of RCA concrete columns is lower than that of NCA concrete columns due to the characteristics of RCA, and whether the existing standards have guidance for the design of RCA columns needs to be verified.

Researchers have explored several methods to improve the performance of NCA and RAC concrete, aiming to

*Corresponding author, Ph.D., Associate Professor,
E-mail: kangtianbei@sjzu.edu.cn
[a] Graduate Student
[b] Ph.D., Professor
[c] Ph.D., Professor

ISSN: 2287-5301 (Print), 2287-531X (Online)

enhance their properties through modification studies. Among these methods, the addition of fibers is an effective approach. Fibers offer a viable alternative to densely arranged transverse bars in column components, which can create weak areas and slightly reduce peak strength (Pour 2022), as they improve the interfacial transition zone and positively impact column performance (Yan *et al*. 2022, Dong *et al*. 2022), though this relies on the assumption of even fiber dispersion under laboratory conditions (Wang *et al*. 2018). Steel fibers enhance the strength and ductility of the concrete, with post-cracking deformation capacity increasing with fiber content (Atea 2019). El-Sayed (2019) demonstrated that recycled steel fibers enhance the ultimate load capacity and deformation characteristics of the beam specimens. However, the poor corrosion resistance of steel fibers limits the long-term performance of components (Zhang and Deng 2018). Polymer fibers, such as polypropylene and glass fiber reinforced polymer, improve concrete tensile and compressive strengths, durability (Kazmi *et al*. 2019, González-Aviña *et al*. 2022). The lateral deformations of glass fiber concrete columns are significant (Xiong *et al*. 2021), this is mainly due to the brittleness and instability of glass fiber reinforced concrete under axial loads. Using glass fiber reinforced polymer bars in reinforcement improved the concrete defection, the patterns of cracks, cracks number of and the failure mode (El-Sayed *et al*. 2021). Recycled metal springs in concrete provide compressive strength 2–3 times greater than steel or polypropylene fibers at 25°C to 900°C (Pachideh *et al*. 2018). Carbon fiber reinforced polymer significantly improves beam stiffness but is prone to sudden brittle failure (Ahmad *et al*. 2010). At the same time, Concrete reinforced with cement slurry injected CFRP composite cladding system has excellent stiffness, strength, ductility, energy dissipation capacity and service performance recovery ability in fire, which is comparable to or even higher than that of undamaged concrete. (Usman *et al*. 2021). Compared to newly manufactured fibers, Zhou *et al*. (2022), Kang *et al*. (2022b) and Wang *et al*. (2000) proposed to use waste fiber (WF) to reinforced RCA concrete. When the replacement rate of RCA is 50%, the incorporation of waste fibers can enhance the compressive strength by 5%-10%, and increased the splitting tensile strength by 12%-15%.

Based on existing research on fiber-reinforced concrete columns, this study investigates the compressive behavior of RCA concrete columns incorporating WFs. According to different fiber lengths, volume fractions of WFs,replacement rates of RCAs, slenderness ratios, and eccentricities, 17 waste fiber recycled concrete (WFRC) columns were constructed. These five variables were systematically analyzed to evaluate their effects on the longitudinal compressive performance of the specimens. The influence of each variable on the structural behavior of the columns is discussed in detail below.

2. Experimental program

2.1 Materials

Ordinary Portland cement (P.O. 42.5) was used in this study. The fine aggregates were natural river sand with a fineness modulus of 2.8, water content of 4.14%, and apparent density of 2620 kg/m^3. The coarse aggregates consisted of NCAs and RCAs. The NCAs are crushed stones with continuous grading with a particle size of 5–25 mm. RCAs were made from waste concrete obtained from the laboratory of Shenyang Jianzhu University, with a strength grade of C40 and a particle size of 5–25 mm. The coarse aggregates properties, as per the Chinese standard GB/T 50081, are listed in Table 1, and the grading curve of the aggregates is shown in Fig. 1 (Zhou *et al*. 2022).

Table 1 Properties of coarse aggregates

Type	Apparent density (kg/m^3)	Bulk density (kg/m^3)	Water absorption (%)	Crushing index (%)
RCAs	2214	1276	4.36	16
NCAs	2690	1535	1.12	6.4

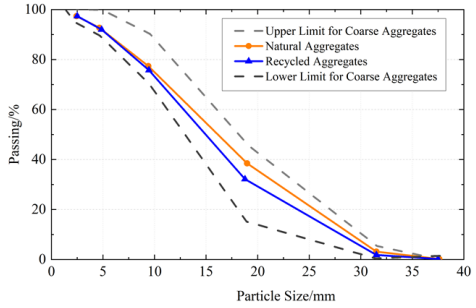

Fig. 1 Coarse aggregates gradating curves

Fig. 2 Preparation of WFs

Table 2 Mixture proportion and specimen designing

Specimen ID	Cement (kg/m^3)	Sand (kg/m^3)	NCAs (kg/m^3)	RCAs (kg/m^3)	Volume fraction of WFs (%)	Length of WFs (mm)	Water (kg/m^3)	l	e (mm)
NC0-19-0.12-5-60	390	709	1156	0	0.12	19	195	5	60
RC50-19-0.12-5-60	390	709	578	578	0.12	19	205	5	60
RC100-19-0.12-5-60	390	709	0	1156	0.12	19	215	5	60
RC50-12-0.12-5-60	390	709	578	578	0.12	12	205	5	60
RC50-30-0.12-5-60	390	709	578	578	0.12	30	205	5	60
RC50-19-0.08-5-60	390	709	578	578	0.08	19	205	5	60
RC50-19-0.16-5-60	390	709	578	578	0.16	19	205	5	60
RC100-19-0.12-2-60	390	709	0	1156	0.12	19	215	2	60
RC100-19-0.12-8-60	390	709	0	1156	0.12	19	215	8	60
RC50-19-0.12-5-30	390	709	578	578	0.12	19	205	5	30
RC50-19-0.12-5-0	390	709	578	578	0.12	19	205	5	0
RC50-19-0.12-2-0	390	709	578	578	0.12	19	205	2	0
RC50-19-0.12-8-0	390	709	578	578	0.12	19	205	8	0
NC0-0-0-2-60	390	709	1156	0	0	0	195	2	60
NC0-0-0-5-60	390	709	1156	0	0	0	195	5	60
NC0-0-0-8-60	390	709	1156	0	0	0	195	8	60
RC50-19-0.12-5-30 (Spare part*)	390	709	578	578	0.12	19	205	5	30

*Spare parts: spare part in this working condition

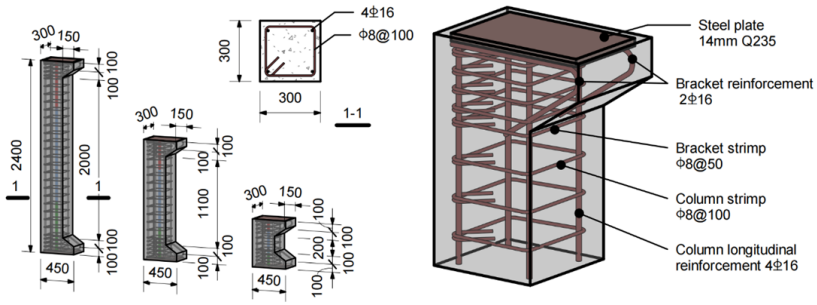

Fig. 3 Specimen reinforcement (The unit in the figure is mm)

WFs originate from artificially treated waste carpets and their main components are polyethylene fibers. After crushing and cleaning, the waste carpet was made into 12, 19, and 30 mm long fibers, as shown in Fig. 2, which were mixed with concrete according to the volume fraction of the specimens.

2.2 Mixture proportions

The material mixtures of the samples are listed in Table 2. The design concrete strength of this experiment was C40, the water–cement ratio was 0.5, and the sand ratio was 38%. The mix proportion design was based on the free water–cement ratio.

There were five variables in this experiment: replacement rate of RCAs (0%, 50%, and 100%), volume fraction of WFs (0%, 0.08%, 0.12%, and 0.16%), length of WFs (12 mm, 19 mm, and 30 mm), initial eccentricity e (0 mm, 30 mm, and 60 mm), and slenderness l (2, 5, and 8).

2.3 Specimen preparation

Considering the actual experiment conditions, the column ends were adjusted during the design of the specimens. The specific sizes and reinforcements of the specimens are shown in Fig. 3. The steel skeleton and the specimen with expired curing are shown in Figs. 4 and 5.

① The rigidity of the two-column ends of the specimen were increased. ② In the specimen design, considering eccentric compression, the column end was designed as a bracket. ③ To ensure that the failure of the specimen occurred at the mid-span of the column during loading, two 14 mm thick Q235 steel plates were embedded at the column end during the design of the specimen, and four 16 mm diameter HRB335 hot-rolled steel bars were welded at the middle of the steel plate. The anchorage length was 20 mm to prevent the warping and deformation of the steel plate during loading. The dimensions of the column section were 300 × 300 mm.

Fig. 4 Steel skeleton

Fig. 5 Specimens

In this experiment, HRB335 hot-rolled ribbed bars with a diameter of 16 mm were selected as the longitudinal load-bearing reinforcement for all concrete columns, and 90° hooks with a length of 14 mm were made at the column ends. HPB235 hot-rolled plain round bars with a diameter of 8 mm were selected as stirrups, and 135° hooks were fabricated during binding. The properties of the steel bars are listed in Table 3. The spacing between the stirrups in the non-densified area was 100 mm. To ensure that the column end had sufficient rigidity and that no local compression failure occurred at the column end, the spacing of the stirrups at the bracket at the column end was 50 mm.

2.4 Specimen loading

For axially compressed columns, the plate loading can be performed directly using a press. The knife hinges should be placed at the upper and lower ends of the specimen to ensure that the upper and lower ends are hinged. The hinged mode and test loading arrangement of the WFRC columns are shown in Fig. 6. Graded loading was applied according to the precalculated ultimate bearing capacity. Before the column started to crack, 20% of the ultimate bearing capacity at each stage was used for loading. The cracking load of a column was recorded. When the load reached 90% of the pre-calculated ultimate bearing capacity, it was halved, and approximately 10% of the ultimate bearing capacity was used for each stage to accurately measure the ultimate bearing capacity of the column. When the column approached failure, it was loaded continuously and slowly until the specimen was damaged. During the test loading process, the load was held for approximately 2 min after each level of loading, and all data were recorded after the readings of the data acquisition

Table 3 Properties of steel bars

Type	Tensile strength (MPa)	Compressive strength (MPa)	Yield strength (MPa)
HPB235	210	210	235
HRB335	300	300	330

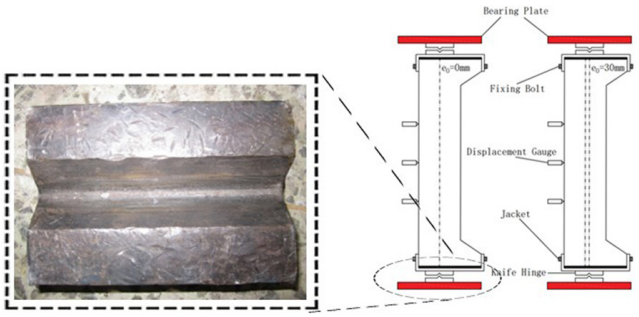

Fig. 6 Loading device

system were stable. The loading time of each specimen was approximately 1 h.

According to the Chinese Standard GB50152-2012, the specimen can be considered to have reached the limit state of the bearing capacity if one of the following signs appears during the test loading. ① The stress of tensile reinforcement reaches the yield strength, and the tensile strain reaches 0.01. ② The lateral deformation reaches 1/50 of the specimen height. ③ The concrete in the compression zone is crushed.

2.5 Data acquisition

Eleven concrete strain gauges were arranged in the mid-span of the WFRC column. Among them, three were arranged on the tension and compression sides, and five were uniformly arranged along the height of the cross-section. On the reinforcement skeleton of the WFRC column, a reinforcement strain gauge was set at the mid-span section of each longitudinal stress reinforcement 10 cm away from the mid-span. A steel bar strain gauge was pasted around the three stirrups in the mid-span section. The position and quantity of the steel bar strain gauge placed at the middle of the longitudinal bar of the axial compression column and the three stirrups at the mid-span are the same as those of the eccentric column. Additionally, a steel bar strain gauge was pasted on the upper and lower 1/4 sections. One displacement meter was placed at 1/4, 1/2, and 3/4 height of the specimen. The distributions of concrete, reinforcement strain gauge, and displacement meter are shown in Fig. 7.

The crack tester used in this test is the PTS-E40 comprehensive crack tester (as shown in Fig. 8). The width measurement range is 0.01~2.1mm, and the depth measurement range is: 10~400 mm, the user can directly read the crack width or depth test value from the LCD screen of the host. The rebar and concrete strain gauges and displacement gauges are connected to the DH3816 static resistance strain gauge through wires (as shown in Fig. 9), and the data measured in the test can be automatically

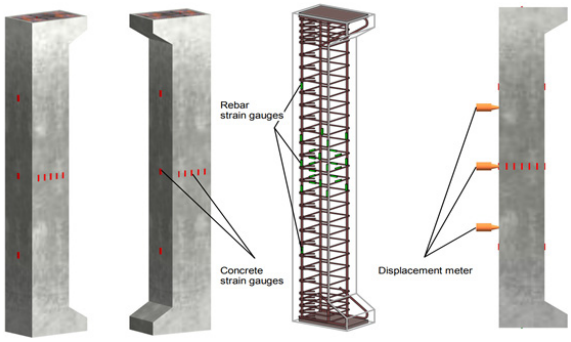

Fig. 7 Position of strain gauge and displacement gauge

collected by the static resistance strain gauge.

3. Experimental phenomena

The three axial compression columns in this test have common characteristics during the stress process. In the initial loading phase, due to the better bond between the concrete and reinforcement, both the load and lateral deformation at mid-span were minimal. Consequently, the column remained in an elastic working stage. When a load

Fig. 8 The crack instrument

Fig. 9 The static resistance strain gauge

(a) Specimen RC50-19-0.12-5-0

(b) Specimen RC50-19-0.12-5-30

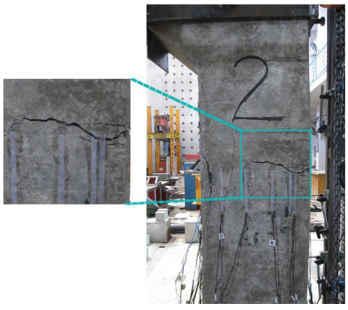

(c) Specimen RC50-19-0.12-5-60

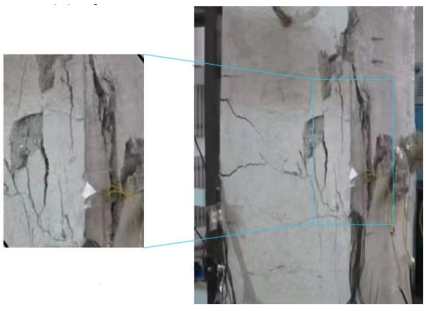

(d) Specimen NC0-0-0-5-60

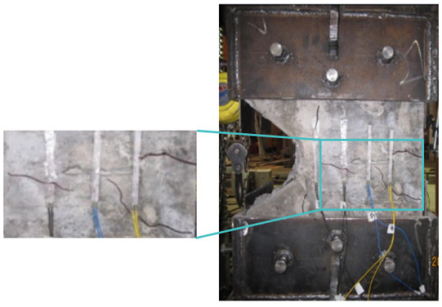

(c) Specimen RC50-19-0.12-5-60

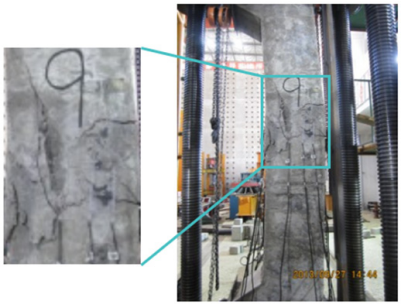

(d) Specimen NC0-0-0-5-60

Fig. 10 Specimen damage pattern

was applied, slight longitudinal cracks first appeared in or near the mid-span of the column. As the loading continued, the longitudinal cracks quickly crossed and extended along the loading direction. When the load approached the ultimate bearing capacity, the concrete at the mid-span section crushed or peeled off. The column lost its bearing capacity, and the test ended. The failure was an obvious brittle failure, and there was little difference between the cracking and failure loads.

Specimen RC50-19-0.12-5-0 (e_0 = 0 mm) is taken as an example to illustrate: in the initial phase of loading, it is in the elastic stage, and there is no crack and no significant change. When the load is loaded to 1871 kN, the first vertical crack appears at the distance of 15 cm from the middle section of the span, and the crack width is about 0.03 mm and the length is about 7 cm. When the load is increased to 2700 kN, the rebar strain at the mid-span section reaches 2265 με, and the rebar begins to yield. With continuous loading, the specimen began to enter the yield phase. As the load increases, the cracks begin to extend to the midspan section and cross rapidly. When the load continued to increase to 2916 kN, the concrete at the mid-span section was crushed, obvious convex appeared, the concrete spall off, and the specimen lost its load-bearing capacity. The failure modes are illustrated in Fig. 10(a).

For a column with e_0 = 60 mm, taking Specimen RC50-19-0.12-5-60 (Fig. 10(c)) as an example, the first transverse crack with a length of about 3 cm appears in the midspan cross-section tension region when the load is loaded to 1246 kN. As the load continues to increase, the number of lateral cracks in the tension area increases, and with the increase of load, the width of the previously appeared cracks gradually widens, and there is a tendency for these cracks to extend outwards. When it was close to failure, the transverse crack in the middle of the span turned into an oblique crack and extended to the compression area, the width of the crack increased sharply, the concrete in the compression area began to fall off, and finally peeling off from the specimen, and the specimen was damaged. At this time, the failure load is 2004 kN, the compressive strain of the concrete in the compression area before the failure is 1622 με, and the strain value of the reinforcement in the tension area is 1483 με. At this time, the reinforcement has been close to yield but still not yield. Additionally, the specimen with e_0 = 60 mm (Fig. 10(c)) cracked and yielded significantly earlier than that with e_0 = 30 mm (Fig. 11(b)).

From comparing the cracking and failure loads between specimen NC0-0-0-5-60 (Fig. 11(d)) and RC50-19-0.12-5-60, it can be concluded that the cracking and failure loads of the WFRC column were lower than those of the NC column, indicating that the strength of the WFRC column was slightly worse than that of the NC compression column.

Since the failure patterns and phenomena of columns with different fiber lengths and different fiber incorporation amounts are basically the same in this test, the failure phenomena of each specimen are not described here. The failure pattern of the specimen with slenderness ratio 2 and slenderness ratio 8 are illustrated in Figs. 10(e)-(f).

After the concrete was shed, we observed on the fracture surface that the dispersion of WFs in the concrete was

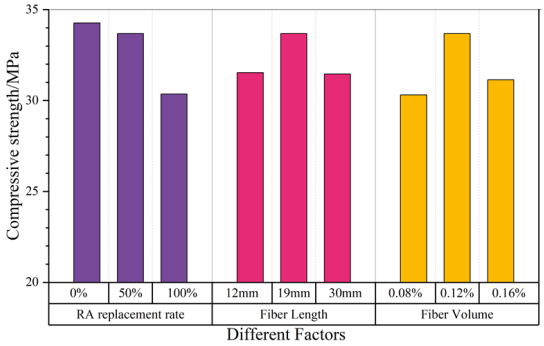

Fig. 11 Compressive strength with different influence factors

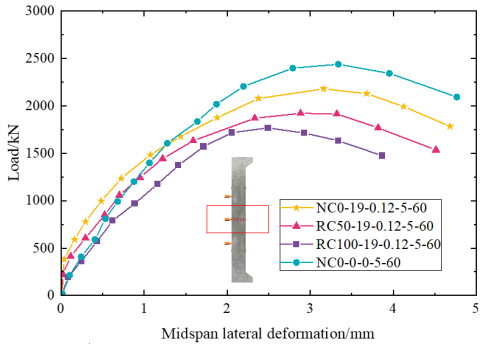

Fig. 12 Load–mid-span lateral deformation curve of replacement rate of RCAs

relatively uniform, and only a small number of WFs appeared to be agglomerated. The fibers at the fracture surface were generally pulled off rather than pulled out, indicating the relatively good bonding performance of the fibers to the concrete. In the process of specimen damage by compression, the fiber consumes its own energy and plays a strengthening role. Thus, the incorporation of fibers played a positive role in changing the damaged form of concrete, and the fibers between cracks effectively prevented the expansion and extension of cracks, restricted the penetration of cracks between concrete components, and prevented the rapid widening of concrete cracks.

4. Results and discussion

4.1 Mechanical properties of WFRC

As shown in Fig. 11, when the volume fraction and WFs length were at the same level, the compressive strength decreased with an increase in the RCA replacement rate. When the replacement rates of the RCA were 50% and 100%, they were 1.72% and 11.41% lower, respectively, than when the replacement rate of RCA was 0%. When the replacement rate of RCA was fixed, the compressive strength first increased and then decreased with an increase in WF length. The compressive strength of the specimen with the WF length of 19 mm was 6.82% higher than that with 12 mm WFs. When the WF length was 30 mm, the

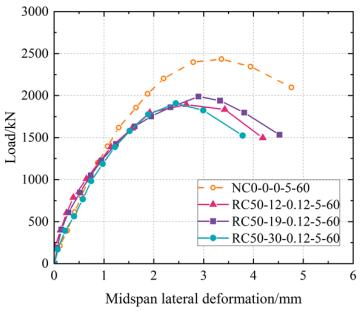

(a) WF Length

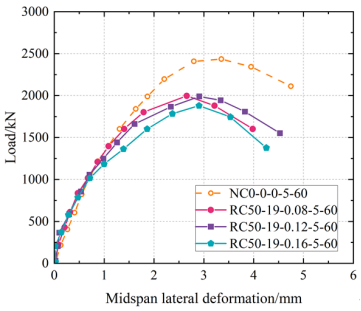

(b) WF volume fraction

Fig. 13 Load–mid-span lateral deformation curve of WFs

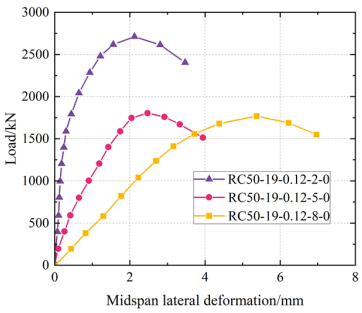

Fig. 14 Load–mid-span lateral deformation curve of l

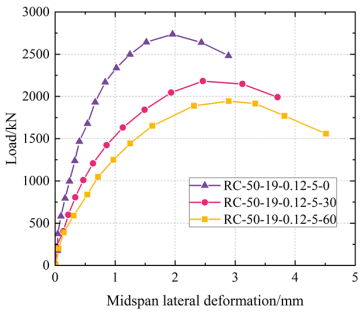

Fig. 15 Load–mid-span lateral deformation curve of e

compressive strength of the specimen was 6.59% lower than that of the specimen with a WF length of 19 mm. The same rule was also observed for the change in the WF volume fraction. When the WF volume fraction was 0.12%, the compressive strength of the specimen was 11.12% higher than that at 0.08%. When the volume fraction of WFs was increased to 0.16%, the compressive strength decreased by 7.54% compared to that with 0.12%. This may be due to the agglomeration of fibers caused by excessive fibers, resulting in the creation of weak areas in the concrete.

4.2 Load–mid-span lateral deformation

The load–mid-span lateral deformation curves obtained by changing the replacement rate of RCAs is shown in Fig. 12. When the replacement rates of the RCAs are different, the lateral deformation of the mid-span section of the column increases with an increase in the replacement rate of RCAs. When the specimen was close to failure, the lateral deformation of the mid-span section increased greatly with the decrease in the replacement rate of the RCAs. Regardless of the RCA replacement rate, the lateral deformation of the WFRC column was generally more significant than that of the NC column, indicating that the ductility of WFRC was more robust than that of NC. This may be because there are many defects and micro-cracks on the surface of RCA, and a large amount of hardened cement paste is attached to its surface. Thus, RCA cannot be as dense as NCA and mortar in NC, the strength of RCA is low, and its ductility is good accordingly.

The lateral deformation diagrams of the WFRC columns were compared by changing the length and volume fraction of the WFs (Fig. 13). Compared to the load of column lateral deformation at mid-span, the variation trends of lateral deformation at mid-span of WFRC and NC columns were the same. However, the mid-span lateral deformation of the NC column is generally smaller than that of the WFRC column, that is, the ductility of WFRC is slightly better than that of NC. When the specimen was close to failure, the maximum lateral deformation first increased and then decreased with the increasing WF volume fraction. When the WF content is lower than the threshold, the fibers in the column are pulled out in the compression process, acting as part of the reinforcement to improve the bearing capacity and ductility of the column, the mechanical performance of the column is improved as the increase of the length and volume fraction of WFs. However, when the volume fraction of WFs is more significant than this threshold, the bond strength between the phases in the concrete decreases because of excessive WF content. This decreases the overall stiffness of the concrete and its mechanical performance. As far as the results of this test are concerned, the WFRC column has the most significant improvement when the WF length is 19 mm and the volume fraction is 0.12%.

As shown in Figs. 14 and 15, with an increase in the slenderness ratio and eccentricity, the mid-span lateral deformation of the WFRC column increased under the same load. This is similar to that of the NC column.

4.3 Load–displacement curves

Fig. 16 shows the lateral deformation curves of each WFRC specimen along the height direction under different loads. Because the ends of the compression column were

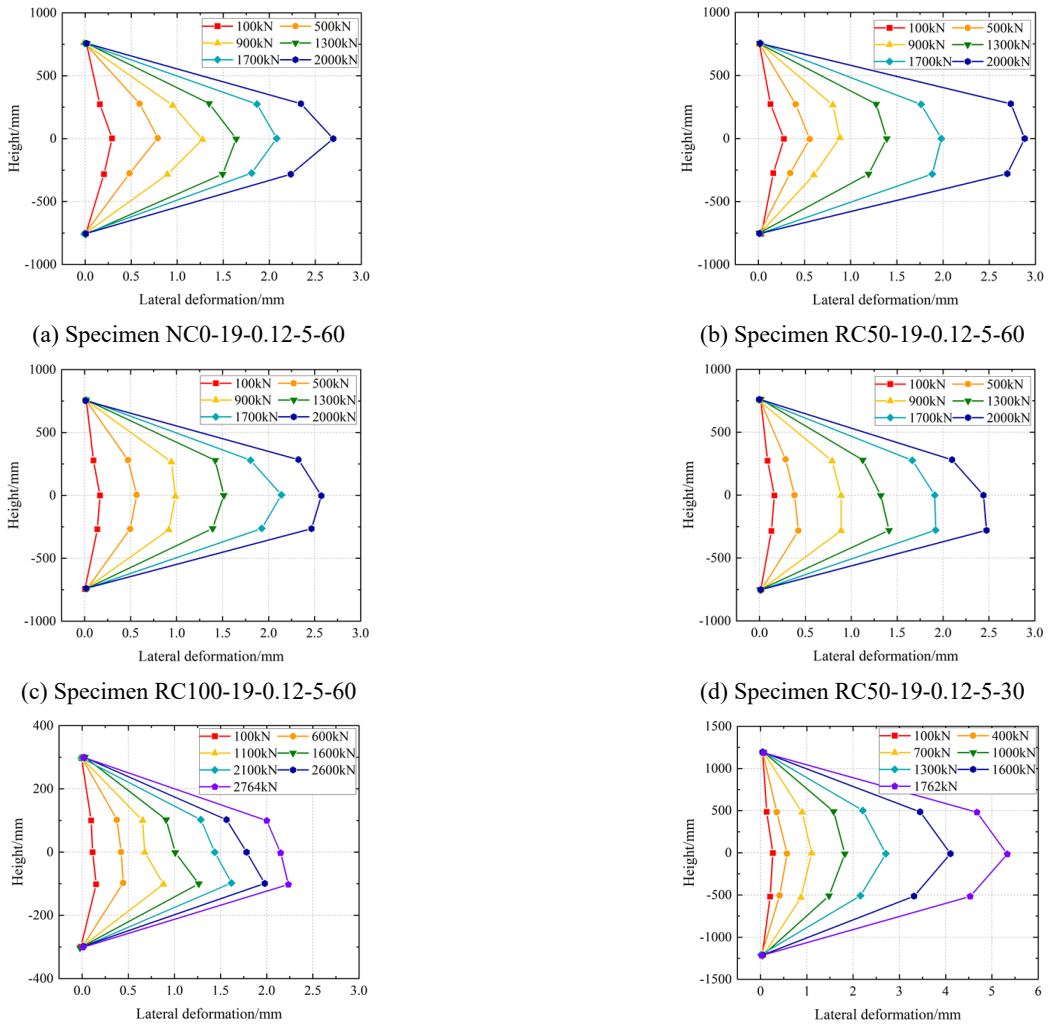

(a) Specimen NC0-19-0.12-5-60

(b) Specimen RC50-19-0.12-5-60

(c) Specimen RC100-19-0.12-5-60

(d) Specimen RC50-19-0.12-5-30

(e) Specimen RC100-19-0.12-2-60

(f) Specimen RC100-19-0.12-8-60

Fig. 16 Load–displacement curves of specimens

connected to the press with knife-edge bearings during loading, both ends could be regarded as hinged. The equation for the lateral deformation curve is as follows

$$y = f \times sin\frac{\pi x}{l_0} \quad (1)$$

where *f* is the stress on the specimen, and l0 is the length of the specimen. According to Eq. (1), the maximum lateral deformation of the specimen occurred at the mid-span of the compression column during the loading of the WFRC column. As both ends of the specimen were hinged, the lateral deformation values at both ends were zero.

The curve in Fig. 16 shows that the lateral deformation of the WFRC column is sinusoidal, and the maximum value generally appears close to the mid-span, i.e., at 1/2 of the column height. The maximum deformation of some individual specimens appears at 1/3 of the specimen height, which is similar to the conclusion for the NC columns. Three stages of lateral deformation occurred between the WFRC and NC columns. At the beginning of loading, all specimens were in the elastic deformation stage. Because the stress of the specimen was low, the deformation of the concrete was mainly due to the elastic deformation of the RCA and cement-based crystals. The load–lateral deformation curve changed linearly, and the lateral deformation was small. The lateral deformation curves at the mid-span of each specimen coincided. Therefore, before the specimen yielded, the lateral deformation of the WFRC column was similar to that of the NC column under the same load. It can be seen from Figs. 16(a), (b) and (c) that with the increase of the replacement rate of the RCA, the transverse deformation of the column in the middle span increases. Since the ultimate load of the specimen in Fig. 16(c) is 1926 kN, the whole specimen is destroyed when the load is increased to 2000 kN, and the mid-span load is less than that of the NC column.

4.4 Characteristic load

As shown in Fig. 17, when the replacement rates of the RCAs were different, the bearing capacities of the RC columns were linearly related to the replacement rate of RCAs. When the replacement rate of RCAs was 50%, the cracking and ultimate loads decreased by 9.2% and 6.3%, respectively. When the replacement rate of RCAs was

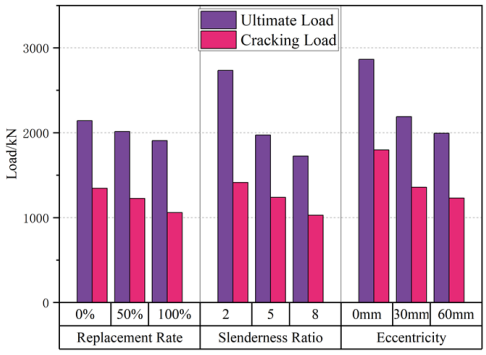

Fig. 17 Relationship of replacement rate, l, e and bearing capacity

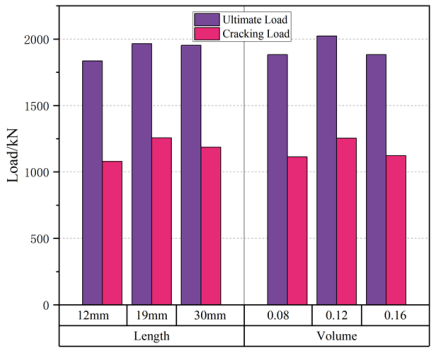

Fig. 18 Relationship of WFs and bearing capacity

100%, the cracking and ultimate loads decreased by 21.3% and 9.6 %, respectively. When the eccentricity is different, as the eccentricity increased, the bearing capacity of the WFRC columns exhibited an apparent downward trend; the smaller the eccentricity, the more noticeable this change.

By comparing and analyzing specimens RC50-12-0.12-5-60, RC50-19-0.12-5-60, RC50-30-0.12-5-60, RC50-19-0.08-5-60, RC50-19-0.12-5-60 and RC50-19-0.16-5-60 we determined the relationship between the length and volume fractions of the WFs and the eccentric compression bearing capacity of the WFRC column. This relationship is illustrated in Fig. 18. It can be observed from Fig. 18 that the bearing capacity of the WFRC columns first increased and then decreased with an increase in WF length. When the length of WFs was 19 mm, the cracking load and ultimate load of the WFRC column reached their maximum values. The bearing capacities of the WFRC columns first increased and then decreased with the increase in the volume fraction of WFs. When the volume fraction of WFs was 0.12%, the bearing capacity was the largest.

According to the provisions of Clause 6.2.15 and Clause 6.2.17 in the code "Code for Design of Concrete Structures" GB50010-2010, the bearing capacity of axially compressed columns and eccentrically compressed columns is calculated respectively. The applicability of the code GB50010-2010 for designing WFRC columns is discussed, and the calculated values and experimental values are listed in Table 4. It can be seen from Table 4 that the experimental values of the bearing capacity of WFRC columns closely approximate the theoretical value, and generally larger than

Table 4 Test value and calculated value of ultimate bearing capacity of each specimen

Specimen ID	Test value (kN)	Theoretical value (kN)	Experimental value /theoretical value
NC0-19-0.12-5-60	2140	2085	1.026
RC50-19-0.12-5-60	2004	1872	1.072
RC100-19-0.12-5-60	1926	1928	1.014
RC50-12-0.12-5-60	1868	1736	1.076
RC50-30-0.12-5-60	1946	1872	1.039
RC50-19-0.08-5-60	1974	1950	1.012
RC50-19-0.16-5-60	1892	1783	1.061
RC100-19-0.12-2-60	2764	2543	1.086
RC100-19-0.12-8-60	1762	1887	0.933
RC50-19-0.12-5-30	1900	2763	1.056
RC50-19-0.12-5-0	2916	3027	1.094
RC50-19-0.12-2-0	3312	2946	0.918
RC50-19-0.12-8-0	2707	2523	1.126
NC0-0-0-2-60	2842	2141	1.062
NC0-0-0-5-60	2274	2309	0.816
NC0-0-0-8-60	1884	2283	0.968
RC50-19-0.12-5-30 (Spare parts)	2216	2085	1.026

the theoretical value. In terms of safety, WFRC columns can be designed and calculated according to the standard calculation formula of NC columns and related regulations. However, due to the limited number of specimens in this experiment, the relationship between the bearing capacity of WFRC and NC column needs further in-depth exploration and research in order to apply WFRC to practical engineering.

4.5 Rebar strain distributions

For axially compressed columns with different slenderness ratios, the strain was uniformly distributed throughout the section, independent of the slenderness ratio. The load–strain curves of the compression reinforcement are shown in Fig. 19. During loading, when the load reached 30%–40% of the ultimate load, the load changed linearly with the steel strain. As the load was continuously applied, the slope of the load–strain relationship curve changed and no longer followed a linear relationship. The specimens failed when the load reached its ultimate value. It can be observed from Fig. 20 that the characteristics of each component in the concrete do not appear initially. The load–reinforcement strain curve of each specimen coincided with that of the NC column. When the load of the specimen reached 1000 kN, the specimen cracked and transverse cracks appeared in the middle of the span. With an increase in the replacement rate of RCAs, the strain of the reinforcement also increased correspondingly and yielded in advance.

By changing the length and volume fraction of WFs, the strain of reinforcement at the mid-span section of the

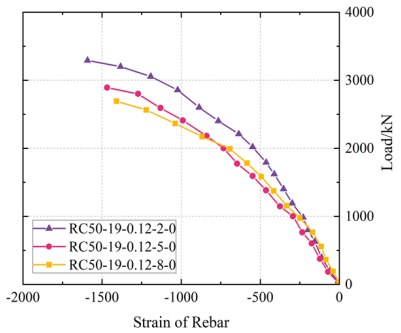

Fig. 19 Load–reinforcement strain curve of axially compressed column

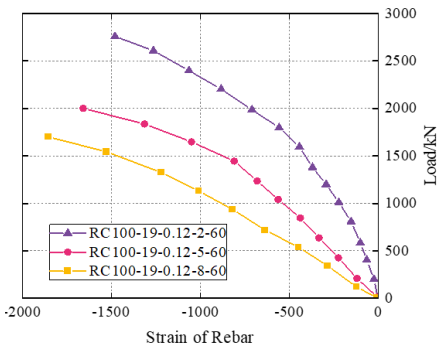

Fig. 22 Load–reinforcement strain curve with different l

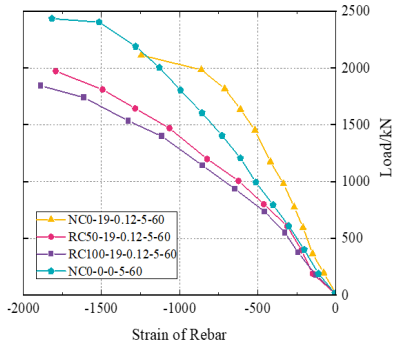

Fig. 20 Load–reinforcement strain curve of different replacement rates of RCAs

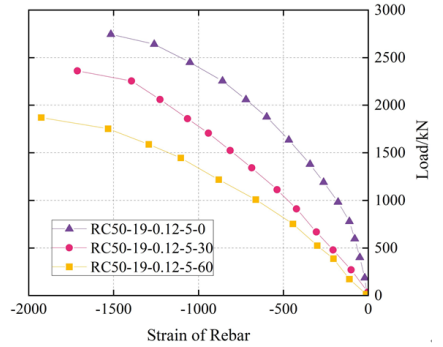

Fig. 23 Load–reinforcement strain curve with different e

WFRC column was analyzed. To facilitate analysis and comparison, the reinforcement strain curve of the NC column is shown in Fig. 21. Under the same load level, the steel bar strain of the specimen with a 12 mm WF length was the smallest, followed by the specimen with a WF length of 30 mm; the steel bar strain of these two specimens was generally more significant than that of the NC columns. The steel bar strain of the specimen with a 19 mm WF length was the largest and increased more significantly than that of the NC columns. The steel strain of the specimen with a WF volume fraction of 0.08% was the smallest, and was close to that of the NC column. The difference between the steel bar strains of specimens with WF volume fractions of 0.12% and 0.16% is small, but they are all greater than the steel bar strain values of the NC columns. In summary, the strain at the mid-span section of the WFRC column first increased and then decreased with an increase in the length and volume fraction of the WFs.

The effects of the different slenderness ratios and eccentricities on the reinforcement strain of WFRC columns were compared. The strain curves are shown in Figs. 22 and 23. With an increase in the slenderness ratio and eccentricity under the same load, the strain of the reinforcement at the mid-span section of the WFRC column increased, which is similar to the change law of the NC column.

From Figs. 19–23, we can see that the reinforcement strains of the WFRC and NC columns share the same characteristics. In the initial stage of loading, there is little difference in the strain of the reinforcement. The strain of the steel bar changed linearly with an increase in load. After

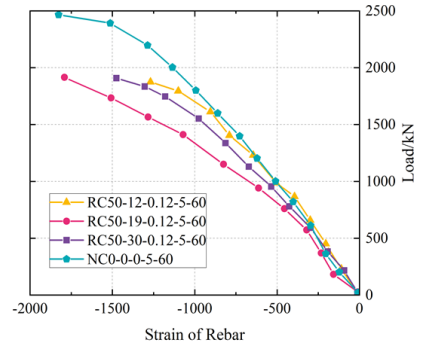

(a) Length of WFs

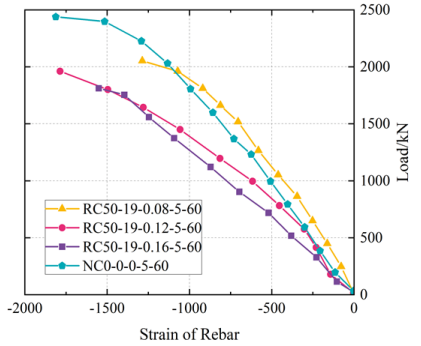

(b) Volume fraction of WFs

Fig. 21 Load–reinforcement strain curve of WFs

the specimen cracked, the curve exhibited a turning point. The strain curves of steel bars in each specimen began to differ to varying degrees until the reinforcement yielded. When the specimen approached failure, the strain in the reinforcement increased rapidly. Because the failure mode of the specimen is a small eccentric compression failure, it is known from the analysis of the reinforcement strain that the reinforcement strain is compressive, and the entire section of the specimen is in compression during the entire stress process.

5. Conclusions

The following conclusions can be drawn from the experimental and analytical investigations:

- The failure processes of WFRC columns were similar to those of NC columns, including the elastic deformation, crack development, reinforcement yield, and failure stages. There was no obvious sign of a small eccentric compression failure, which is a brittle failure.
- The cracking load and ultimate bearing capacity of the WFRC columns decreased as the replacement rate of RCAs increased. The cracking load and ultimate bearing capacity first increased and then decreased with increasing length and volume fraction of WFs. In this test, when the WF length was 19 mm and WF volume fraction was 0.12%, the bearing capacity of the WFRC column was the highest. The mixing of WFs effectively improved the poor ductility of NC and significantly improved the ductility of WFRC columns. Compared with NC columns, WFRC columns exhibited a better bearing capacity when the specimens were close to failure.
- The effects of slenderness ratio and eccentricity on the bearing capacity of WFRC columns were similar to those of NC columns. With an increase in slenderness ratio and eccentricity, the cracking load and ultimate bearing capacity of the specimens decreased. Under axial compression, the cracking load and ultimate bearing capacity of WFRC columns decreased with the slenderness ratio, as observed with NC columns.
- In this experiment, only three specific lengths and incorporation ratios of waste fibers were selected. It is recommended that future research conduct extensive and in-depth investigations into other fiber lengths and incorporation ratios to identify the optimal fiber incorporation ratio. Additionally, this study has only preliminarily examined the mechanical performance of WFRC columns. Further research should explore other structural components, such as walls and joints, to provide a more comprehensive understanding of WFRC.

Acknowledgments

The financial support is gratefully acknowledged. This research was supported by the National Natural Science Foundation of China (no. 52108235), Liaoning Provincial Department of Education Fund (nos. JYTMS20231578; LT2019011), and the open research fund of Shenyang Key Laboratory of Low-carbon Transportation Construction, Maintenance and Operation (no. LJ232410153005 JT-Y24-3). These sources of financial support are gratefully acknowledged.

Data availability

The datas used to support the findings of the study are included within the manuscript.

Conflicts of interest

No potential conflict of interest was reported by the authors.

References

Ahmad, S., Shah, A., Nawaz, A. and Salimullah, K. (2010), "Shear strengthening of corbels with carbon fibre reinforced polymers (CFRP)", *Materiales de Construcción*, **60**(299), 79-97. https://doi.org/10.3989/mc.2010.50009

Atea, R.S. (2019), "A case study on concrete column strength improvement with different steel fibers and polypropylene fibers", *J. Mater. Res. Technol.*, **8**(6), 6106-6114. https://doi.org/10.1016/j.jmrt.2019.10.005

Dong, J.F., Wang, Q.Y., Guan, Z.W. and Chai, H.K. (2022), "High-temperature behaviour of basalt fibre reinforced concrete made with recycled aggregates from earthquake waste", *J. Build. Eng.*, **48**, 103895. https://doi.org/10.1016/j.jobe.2021.103895

El-Sayed, T.A. (2019), "Flexural behavior of RC beams containing recycled industrial wastes as steel fibers", *Constr. Build. Mater.*, **212**, 27-38. https://doi.org/10.1016/j.conbuildmat.2019.03.311

El-Sayed, T.A. and Algash, Y.A. (2021), "Flexural behavior of ultra-high performance geopolymer RC beams reinforced with GFRP bars", *Case Stud. Constr. Mater.*, **15**, 00604. https://doi.org/10.1016/j.cscm.2021.e00604

Gao, D., Li, W., Pang, Y. and Huang, Y. (2021), "Behavior analysis and strength prediction of steel fiber reinforced recycled aggregate concrete column under axial compression", *Constr. Build. Mater.*, **290**, 123278. https://doi.org/10.1016/j.conbuildmat.2021.123278

González-Aviña, J.V., Juárez-Alvarado, C.A., Terán-Torres, B.T., Mendoza-Rangel, J.M., Durán-Herrera, A. and Rodríguez-Rodríguez, J.A. (2022), "Influence of fibers distribution on direct shear and flexural behavior of synthetic fiber-reinforced self-compacting concrete", *Constr. Build. Mater.*, **330**, 127255. https://doi.org/10.1016/j.conbuildmat.2022.127255

Kang, T.B., Liu, Y., Zhou, J.H., Wang, F.C. and Zhang, Y.C. (2022a), "Chloride transport performance of waste fiber recycled concrete under dry-wet cycles", *J. Build. Mater.*, **25**(4), 389-394. https://doi.org/10.3969/j.issn.1007-9629.2022.04.009

Kang, T., Li, S., Jin, L., Wu, X., Zhou, J., Zhang, Y. and Liang, Y. (2022b), "Size effect on compressive behaviors of waste fiber-reinforced recycled aggregate concrete", *Eur. J. Environ. Civil Eng.*, **26**(15), 7811-7824. https://doi.org/10.1080/19648189.2021.2011424

Kazmi, S.M.S., Munir, M.J., Wu, Y.F., Patnaikuni, I., Zhou, Y. and Xing, F. (2019), "Axial stress-strain behavior of macro-synthetic fiber reinforced recycled aggregate concrete", *Cement Concrete Compos.*, **97**, 341-356.

https://doi.org/10.1016/j.cemconcomp.2019.01.005
Liu, C., Fan, J., Bai, G., Quan, Z., Fu, G., Zhu, C. and Fan, Z. (2019), "Cyclic load tests and seismic performance of recycled aggregate concrete (RAC) columns", *Constr. Build. Mater.*, **195**, 682-694. https://doi.org/10.1016/j.conbuildmat.2018.10.078
Ma, H., Bai, H., Zhao, Y., Liu, Y. and Zhang, P. (2019), "Compressive performance of RAC filled GFRP tube-profile steel composite columns under axial loads", *Adv. Concrete Constr., Int. J.*, **8**(4), 335-349. https://doi.org/10.12989/acc.2019.8.4.335
Naran, J.M., Gonzalez, R.E.G., del Rey Castillo, E., Toma, C.L., Almesfer, N., van Vreden, P. and Saggi, O. (2022), "Incorporating waste to develop environmentally-friendly concrete mixes", *Constr. Build. Mater.*, **314**, 125599. https://doi.org/10.1016/j.conbuildmat.2021.125599
Pachideh, G., Majid, G. and Amin, M. (2018), "Performance of concrete containing recycled springs in post-fire conditions", *Proc. Inst. Civil Eng. – Struct. Build.*, **173**(1), 3-16. https://doi.org/10.1680/jstbu.18.00042
Poon, C.S., Shui, Z.H., Lam, L., Fok, H. and Kou, S.C. (2004), "Influence of moisture states of natural and recycled aggregates on the slump and compressive strength of concrete", *Cement Concrete Res.*, **34**(1), 31-36. https://doi.org/10.1016/S0008-8846(03)00186-8
Pour, A.K. (2022), "Experimental and numerical evaluation of steel fibres RC patterns influence on the seismic behaviour of the exterior concrete beam-column connections", *Eng. Struct.*, **263**, 114358. https://doi.org/10.1016/j.engstruct.2022.114358
Shen, W., Liu, Y., Yan, B., Wang, J., He, P., Zhou, C. and Ding, Q. (2017), "Cement industry of China: Driving force, environment impact and sustainable development", *Renew. Sust. Energy Rev.*, **75**, 618-628. https://doi.org/10.1016/j.rser.2016.11.033
Strieder, H.L., Dutra, V.F.P., Graeff, Â.G., Núñez, W.P. and Merten, F.R.M. (2022), "Performance evaluation of pervious concrete pavements with recycled concrete aggregate", *Constr. Build. Mater.*, **315**, 125384. https://doi.org/10.1016/j.conbuildmat.2021.125384
Sunayana, S. and Barai, S.V. (2019), "Performance of fly ash incorporated recycled aggregates concrete column under axial compression: Experimental and numerical study", *Eng. Struct.*, **196**, 109258. https://doi.org/10.1016/j.engstruct.2019.05.099
Usman, M., Yaqub, M., Auzair, M., Khaliq, W., Noman, M. and Afaq, A. (2021), "Restorability of strength and stiffness of fire damaged concrete using various composite confinement techniques", *Constr. Build. Mater.*, **272**, 121984. https://doi.org/10.1016/j.conbuildmat.2020.121984
Wang, R., Gao, X., Zhang, J. and Han, G. (2018), "Spatial distribution of steel fibers and air bubbles in UHPC cylinder determined by X-ray CT method", *Constr. Build. Mater.*, **160**, 39-47. https://doi.org/10.1016/j.conbuildmat.2017.11.030
Wang, Y., Wu, H.C. and Li, V.C. (2000), "Concrete reinforcement with recycled fibers", *J. Mater. Civil Eng.*, **12**(4), 314-319. https://doi.org/10.1061/(ASCE)0899-1561(2000)12:4(314)
Xiong, Z., He, S.H., Kwan, A.K.H., Li, L.G. and Zeng, Y. (2021), "Compressive behaviour of seawater sea-sand concrete containing glass fibres and expansive agents", *Constr. Build. Mater.*, **292**, 123309. https://doi.org/10.1016/j.conbuildmat.2021.123309
Yan, H., Gao, D., Guo, A., Gu, Z., Ji, D. and Zhang, Y. (2022), "Monotonic and cyclic bond responses of steel bar with steel-polypropylene hybrid fiber reinforced recycled aggregate concrete", *Constr. Build. Mater.*, **327**, 127031. https://doi.org/10.1016/j.conbuildmat.2022.127031
Yaragal, S.C., Teja, D.C. and Shaffi, M. (2016), "Performance studies on concrete with recycled coarse aggregates", *Adv. Concrete Constr., Int. J.*, **4**(4), 263-281. https://doi.org/10.12989/acc.2016.4.4.263
Yazdani, M., Kabirifar, K., Frimpong, B.E., Shariati, M., Mirmozaffari, M. and Boskabadi, A. (2021), "Improving construction and demolition waste collection service in an urban area using a simheuristic approach: A case study in Sydney, Australia", *J. Clean Prod.*, **280**, 124138. https://doi.org/10.1016/j.jclepro.2020.124138
Zhang, X. and Deng, Z. (2018), "Experimental study and theoretical analysis on axial compressive behavior of concrete columns reinforced with GFRP bars and PVA fibers", *Constr. Build. Mater.*, **172**, 519-532. https://doi.org/10.1016/j.conbuildmat.2018.03.237
Zhao, M.Z., Geng, Y., Wang, Y.Y. and Hu, J.X. (2022), "Compounding effect and an expanded theoretical model for recycled coarse and fine aggregate concretes under uniaxial loading", *Constr. Build. Mater.*, **320**, 126226. https://doi.org/10.1016/j.conbuildmat.2021.126226
Zhou, J., Jin, L., Qu, J., Sun, H., Kang, T., Yuan, Y. and Liu, Y. (2022), "Experimental Research on Waste Fiber Recycled Concrete Beam-to-Column Joints under Monotonic Loading", *Adv. Mater. Sci. Eng.*, **2022**(1), 2240624. https://doi.org/10.1155/2022/2240624